

Thomas R. Kunson, Joseph J. Sirutis • Ming Zhao • Robert E. Tuleya • Morris Bender •

Introduction:

普遍問題:

- How tropical cyclone activity could be altered by future anthropogenic warming?
- The uncertainties in the patterns of future sea surface temperature (SST) changes can lead also to uncertainties in the associated tropical cyclone projections. (vertical structure of temperature changes)
- Relatively coarse grid global models, such as those used in CMIP3 or CMIP5 usually do not produce very realistic climatological tropical cyclone activity and are particularly deficient at simulating very intense tropical cyclones.

Using a dynamical downscaling approach to investigate the response of tropical cyclones in all basins to a climate change scenario obtained from a multimodal ensemble of CMIP5 models (RCP4.5 scenario).

Data and methods:

- GCMs Models: HiRAM C180 global model (Geophysical Fluid Dynamics Laboratory High Resolution Atmospheric Model, 50-km).
 - based on the availability of sea ice concentration data at the time multimodal ensemble was constructed for earlier study.
- RCM Model: GFDL hurricane model

TABLE 1. Summary of the 13 CMIP5 (Taylor et al. 2012) global climate models used in this study to create the multimodel anomalies in HiRAM (using SST and sea ice concentration). (Expansions of acronyms are available online at <http://www.ametsoc.org/PubsAcronymList>.)

Modeling center (or group)	Model name
Canadian Centre for Climate Modeling and Analysis	CanESM2
Centre National de Recherches Meteorologiques/Centre Européen de Recherche et Formation Avancée en Calcul Scientifique	CNRM-CM5
Commonwealth Scientific and Industrial Research Organization in collaboration with Queensland Climate Change Centre of Excellence	CSIRO-Mk3.6.0
Chinese Academy of Sciences, State Key Laboratory Numerical Modeling for Atmospheric Sciences and Geophysical Fluid Dynamics	FGOALS-g2
NOAA Geophysical Fluid Dynamics Laboratory	GFDL-CM3
NOAA Geophysical Fluid Dynamics Laboratory	GFDL-ESM2G
NOAA Geophysical Fluid Dynamics Laboratory	GFDL-ESM2M
Met Office Hadley Centre	HadGEM2-ES
Atmosphere and Ocean Research Institute (The University of Tokyo), National Institute for Environmental Studies, and Japan Agency for Marine-Earth Science and Technology	MIROC-ESM
Japan Agency for Marine-Earth Science and Technology, Atmosphere and Ocean Research Institute (The University of Tokyo), and National Institute for Environmental Studies	MPI-ESM-LR
Max Planck Institute for Meteorology	MRI-CGCM3
Meteorological Research Institute	NorESM1-M
Norwegian Climate Centre	

Gabriel A. Vecchi • Gabriele Villarini • Daniel Chavas

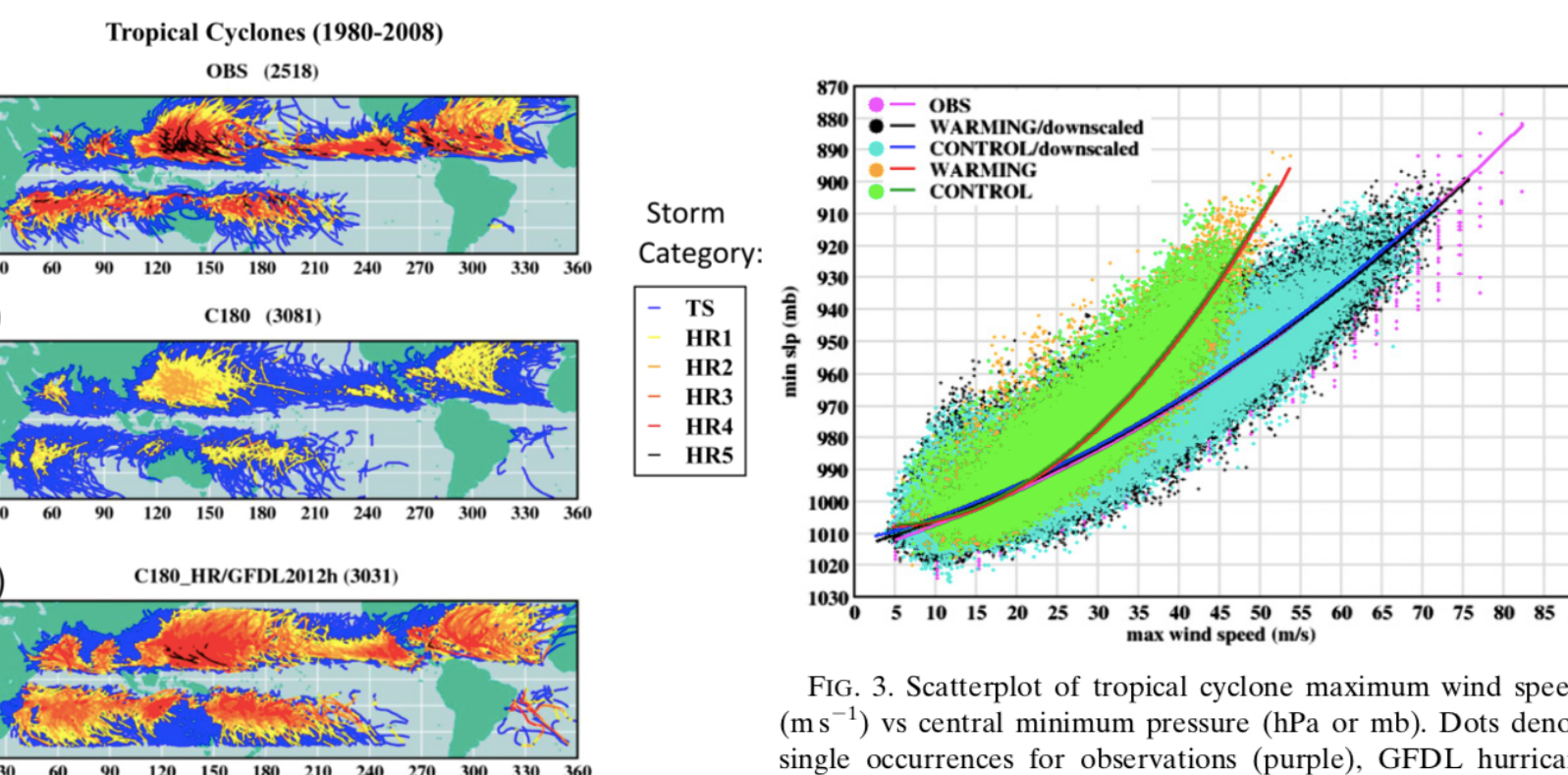


FIG. 1. (a) Tracks of observed tropical cyclones for the years 1980–2008. (b) Simulated tropical cyclone tracks for 1980–2008 obtained using HiRAM C180 running over observed interannually varying SSTs (1980–2008). (c) Simulated tropical cyclone tracks obtained using the GFDL hurricane model to resimulate tropical cyclone cases at higher resolution. These cases in (c) used the HiRAM C180 simulation to provide initial conditions and boundary conditions for the individual storm cases to the higher-resolution model. Storm categories on the Saffir–Simpson scale are depicted by the track colors, varying from tropical storm (blue) to category 5 (black; see legend). The numbers in parentheses above each panel denote the total number of storms found.

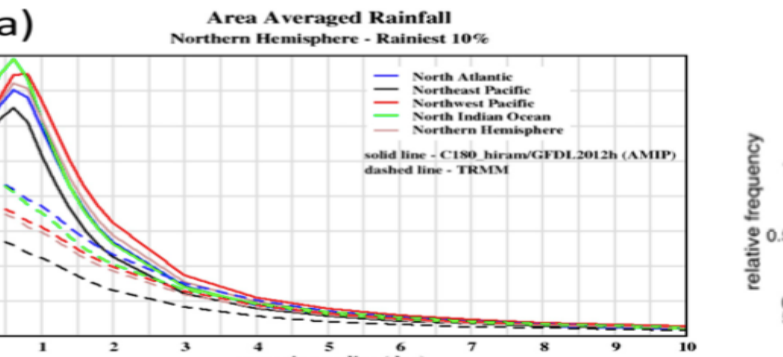


FIG. 4. Profiles of tropical cyclone precipitation rates (mm day^{-1}), averaged from the storm center to the radius indicated on the abscissa (in degrees) based on the lifetime-average precipitation from the 10雨iest tropical cyclones (see text). The curves are compared for observations from TRMM satellite measurements (dashed) and the GFDL hurricane model (solid) for downscaling experiments based initially on HiRAM C180 global atmospheric simulations obtained using observed interannually varying SSTs (1980–2008). Results are shown for the (a) Northern and (b) Southern Hemisphere for various tropical cyclone basins (colors; see legend).

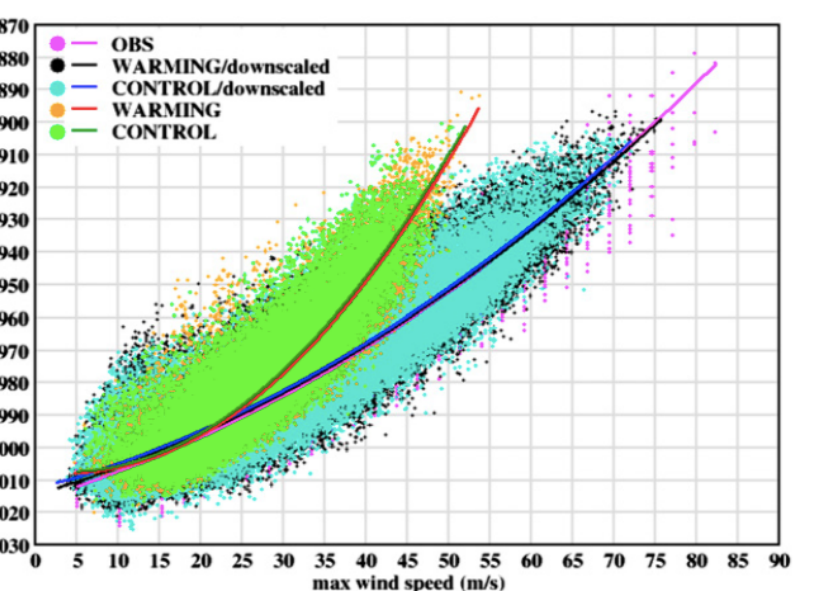


FIG. 3. Scatterplot of tropical cyclone maximum wind speeds (m s^{-1}) vs central minimum pressure (hPa or mb). Dots denote single occurrences for observations (purple), GFDL hurricane model control runs (aqua) and late-twenty-first-century projection runs (black), or HiRAM C180 control runs (green) and late-twenty-first-century projections (orange). Observations are shown by the purple dots and curve. The smooth curves are least squares quadratic best-fit lines through the data for the various cases. Note that the observations are shown for the period 2001–12, while the “Control” simulations shown are based on climatological SST conditions for 1982–2005.

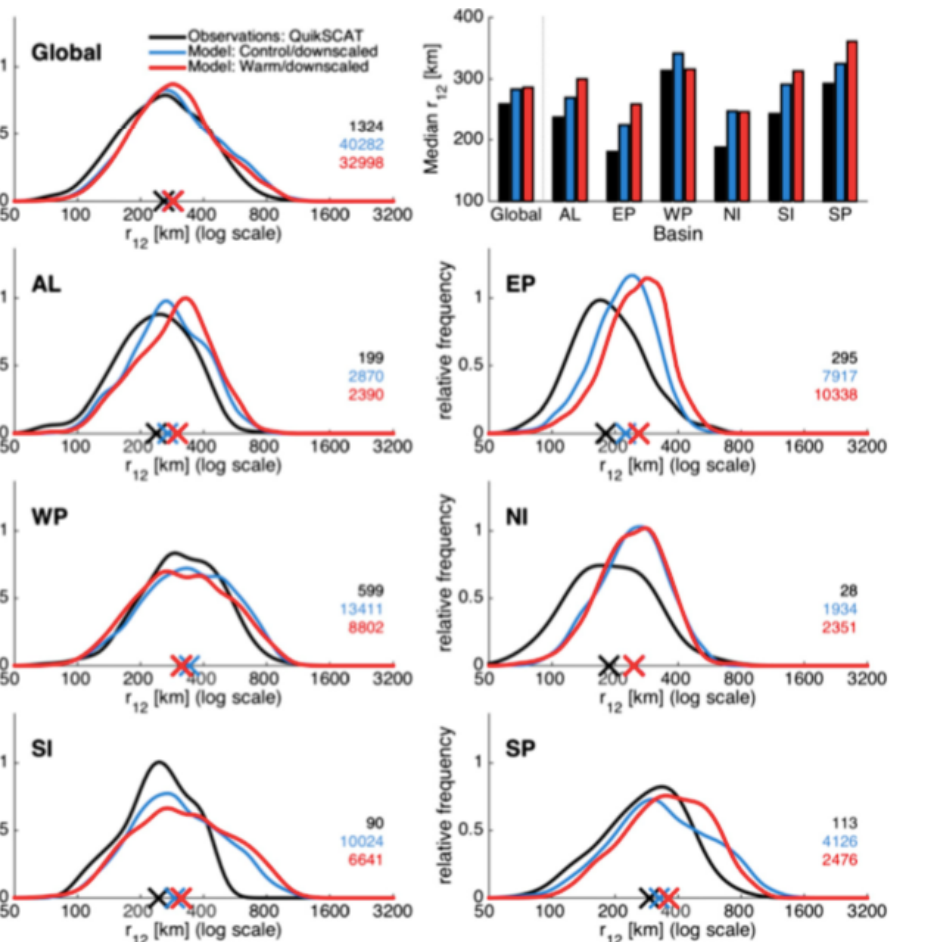


FIG. 5. Relative frequency of tropical cyclone size, globally and for various tropical cyclone basins (AL = North Atlantic; EP = northeast Pacific; WP = northwest Pacific; NI = north Indian; SI = south Indian; SP = southwest Pacific). The size metric, r_{12} , is the radius at which the azimuthal-mean azimuthal wind speed decreases to 12 m s^{-1} . Black curves depict observed estimates based on QuikSCAT satellite measurements; blue and red curves depict distributions based on model simulations for control (present day; blue) or warm climate (late twenty-first century; red) conditions. The “X” marks on each diagram denote median values. The numbers listed on each diagram denote the number of cases analyzed. The top right panel shows the global and interbasin variation of median tropical cyclone sizes for this metric. Control runs are based on climatological SSTs for 1982–2005. See text for further details.

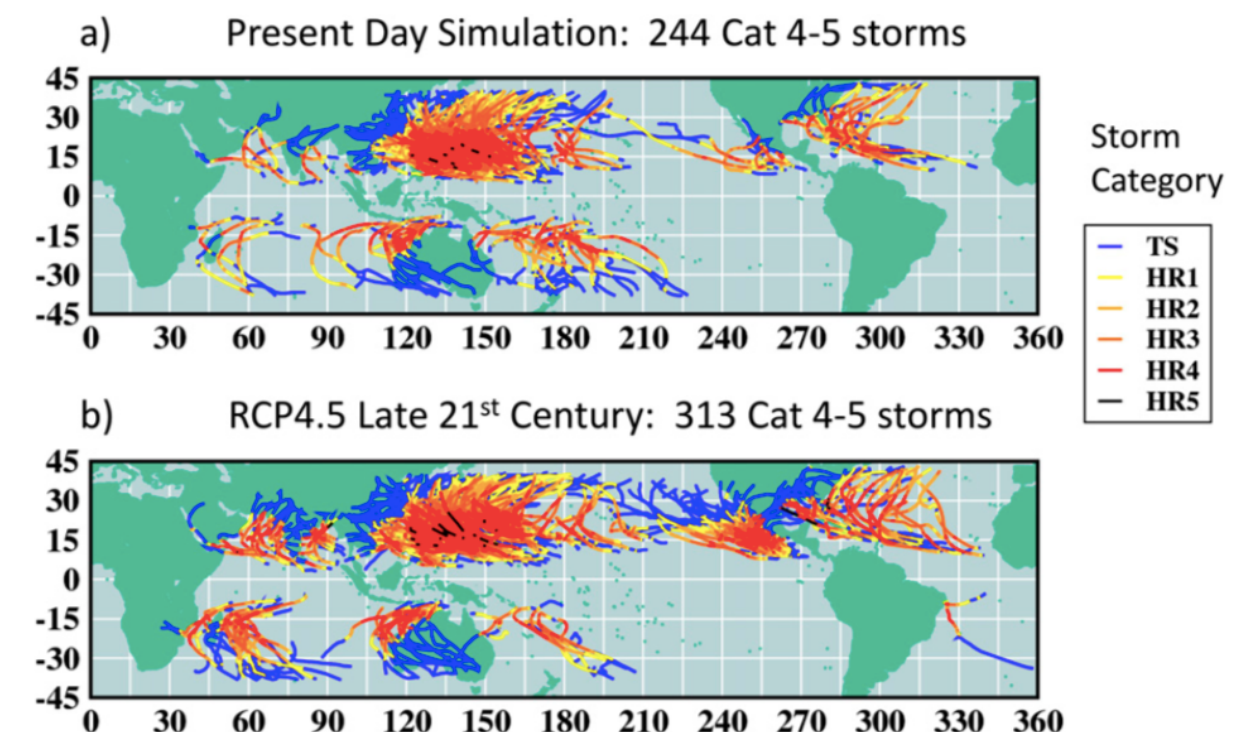


FIG. 7. Tracks of simulated cat 4–5 tropical cyclones for (a) present-day or (b) late-twenty-first-century (RCP4.5; CMIP5 multimodel ensemble) conditions. Simulated tropical cyclone tracks were obtained using the GFDL hurricane model to resimulate (at higher resolution) the tropical cyclone cases originally obtained from the HiRAM C180 global mode. Storm categories or intensities are shown over the lifetime of each storm, according to the Saffir–Simpson scale. The categories are depicted by the track colors, varying from tropical storm (blue) to category 5 (black; see legend).

Conclusions:

- HiRAM C180 fails to capture tropical cyclones with winds of category 4 and 5 intensity, which we believe is important for late-twenty-first-century climate change projection studies.
- Salient features of the late-twenty-first-century projected changes include a substantial reduction in global tropical cyclone frequency (-16%), but an increase in the frequency of the most intense storms (+24% for cat 4-5).
- The increase in projected cat 4-5 occurrence is fairly widespread in the Northern Hemisphere basins. There is also decreased cat 4-5 occurrence projected in some areas, but these are more limited regions—notably the southwest Pacific and eastern Indian Ocean basins, and parts of the northwest Pacific basin.

Introduction:

- Small changes in the mean and standard deviation values can produce relatively large changes in the probability of extreme events.
- The relationship between predictor and predictand is often very complex in nature, and linear regression based methods cannot work very well.

- Pakistan is one of the most vulnerable countries in the world to climate change.

Data and methods:

- Baluchistan is a mountainous, desert and an arid province, located between 30.12°N and 67.01°E .
- Monsoon winds and the western depression are the main sources of rainfall during summer and winter, respectively in the area.
- GCMs: 20 grid points covering the region.

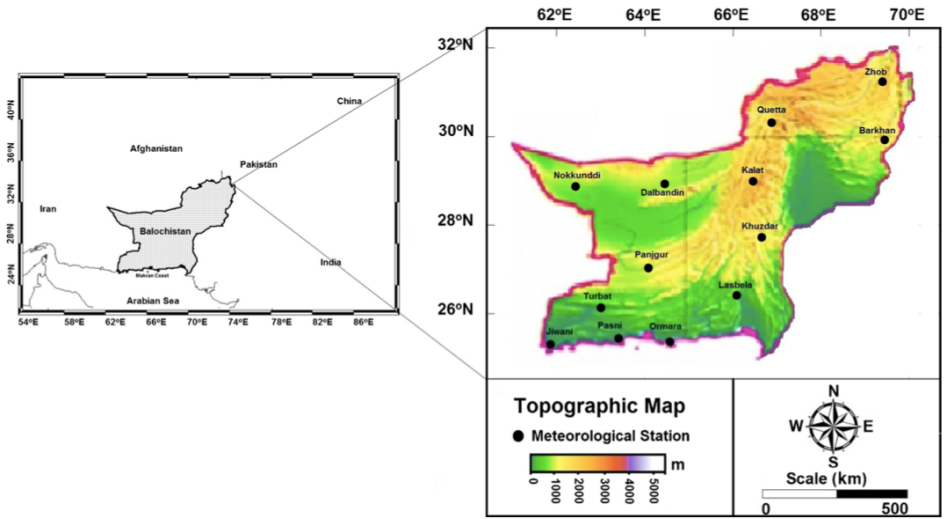


Figure 1. Geographical location and topography of Baluchistan province of Pakistan.

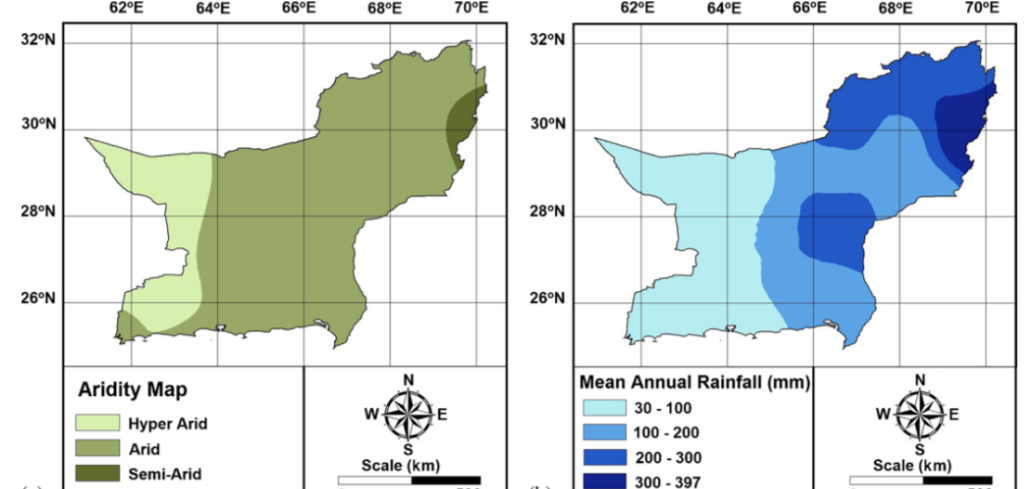


Figure 2. (a) Aridity and (b) mean annual rainfall in Baluchistan.

MLP and PCA:

$$y_k = F \left(\sum_{j=1}^h w_j G(s_i) + b_k \right)$$

$$G(s_i) = \frac{e^{s_i} - e^{-s_i}}{e^{s_i} + e^{-s_i}} \quad s_i = \sum_{i=1}^n w_i x_i$$

PCA: aims to reduce the dimensionality of a dataset of a large number of interrelated variables, while retaining as much as possible of the variation present in the dataset.

- RMSE, r^2 , MBE, NSE (Nash-Sutcliffe model efficiency)
- 1961-1990, 1991-2001

$$\text{NSE} = 1 - \frac{\sum_{i=1}^N (x_{\text{sim}, i} - x_{\text{obs}, i})^2}{\sum_{i=1}^N (x_{\text{obs}, i} - \bar{x}_{\text{obs}})^2}$$

Table 3. Number of principal components and the cumulative variance represented by the selected principle components in each month.

Month	No. of components	Cumulative variance (%)
January	24	98.94
February	25	99.17
March	25	98.95
April	25	98.86
May	25	98.87
June	26	98.86
July	24	98.91
August	24	98.70
September	24	98.71
October	24	98.88
November	25	99.03
December	23	98.90

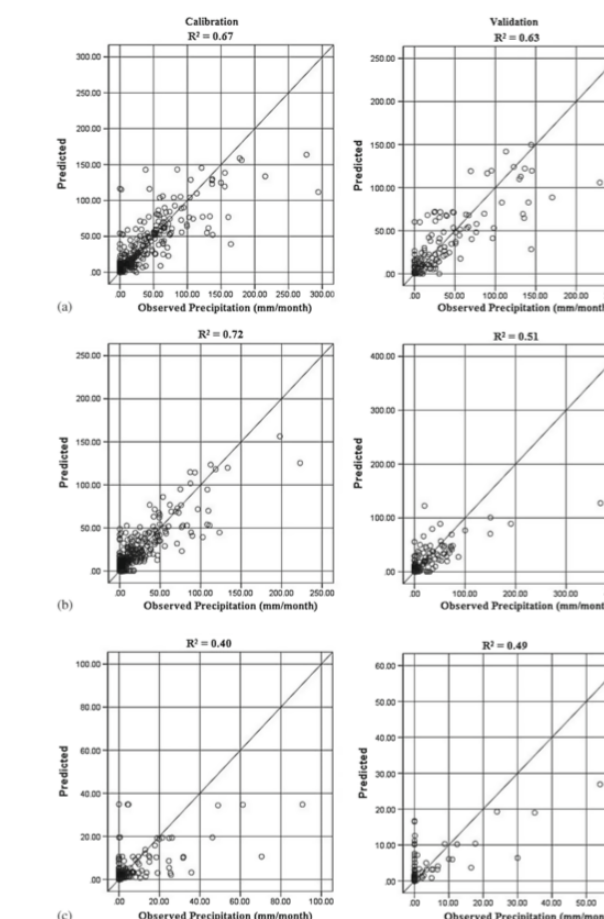


Figure 5. Observed and downscaled rainfall time series at (a) Barkhan (semi-arid), (b) Khuzdar (arid), and (c) Nokkundi (hyper-arid) stations.

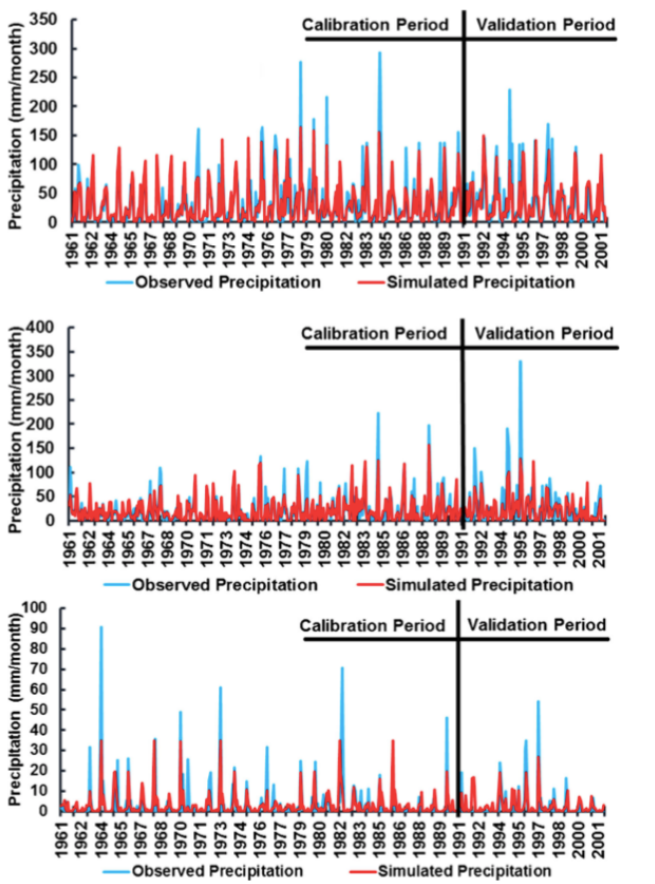


Figure 8. Scatter plot of observed and downscaled rainfall at (a) Barkhan (semi-arid), (b) Khuzdar (arid), and (c) Nokkundi (hyper-arid) stations.

Conclusions:

- MLP neural network was capable to downscale precipitation in most of the stations in the study area satisfactorily.

- MLP neural network can be used downscaling monthly rainfall in such regions.

Future studies:

- The spatial domain covered by 20 grid points may not be enough to capture the regional synoptic circulation patterns that contribute to the anomalous rainfall pattern in arid region.
- Random selection of training and testing of data can be used to improve the efficiency of downscaling model.
- Other data mining and predictor selection approaches can be used to assess the performance of different methods in downscaling rainfall in arid regions.

Report

2020.11.04

張慕琪

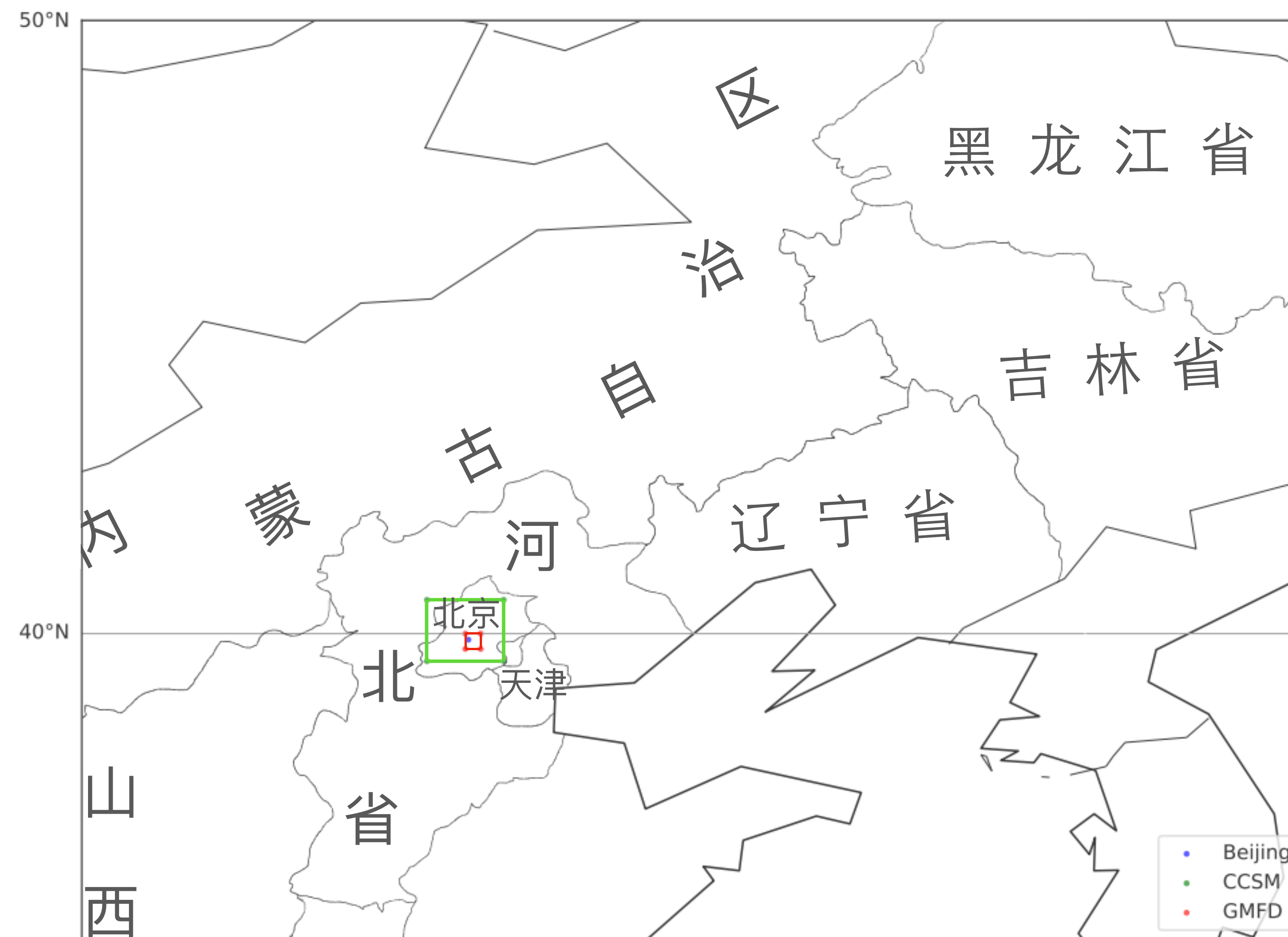


图1 模式数据和观测数据分辨率对比
Fig. 1 The Comparison of CCSM4 and GMFD's resolution

输入层

隐藏层1

隐藏层2

输出层

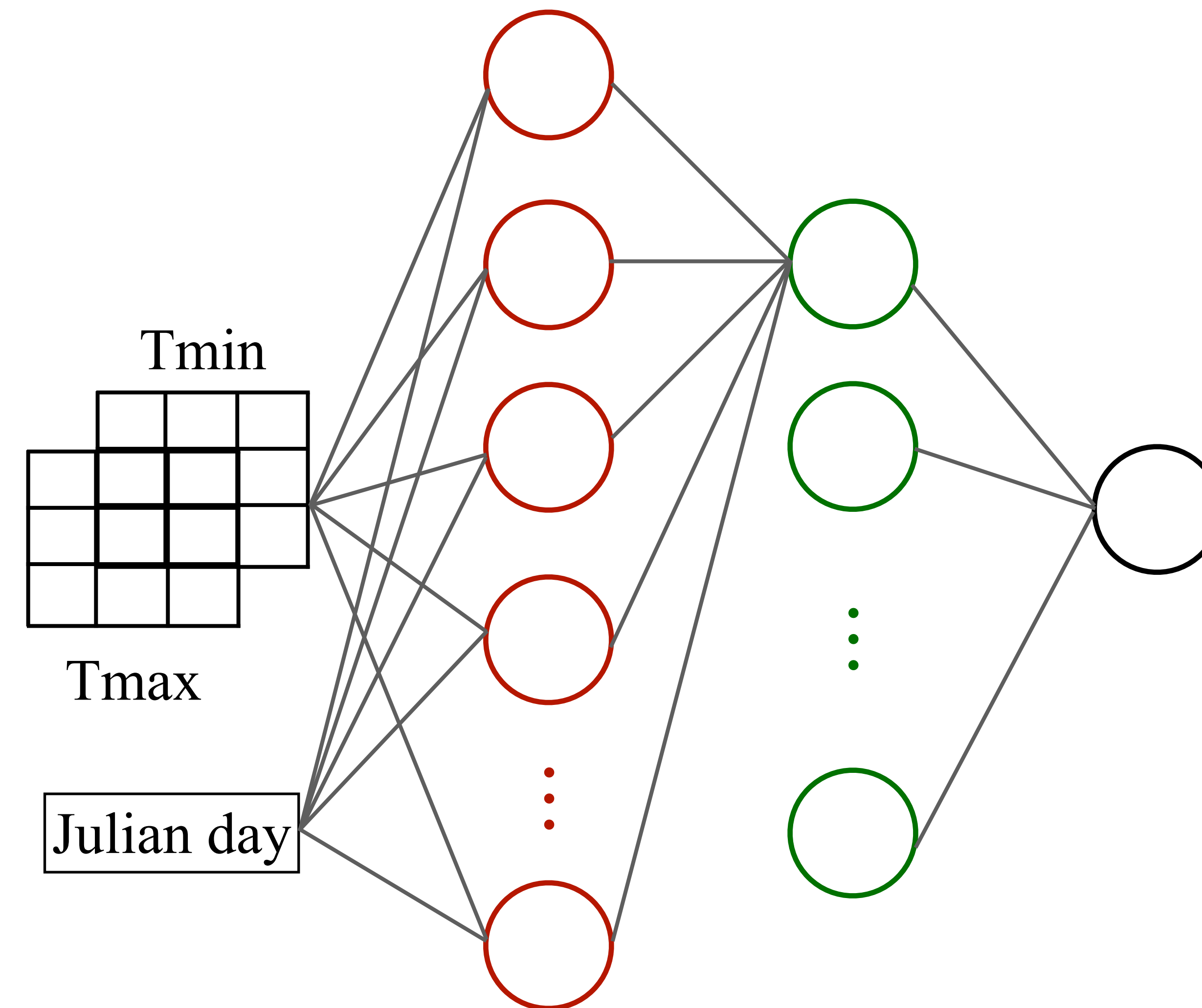


图2 多层感知器网络结构

Fig. 2 The Structure of MLPRegressor

图3 方法比较（北京）

Fig. 4 The Comparison of different methods (Beijing)

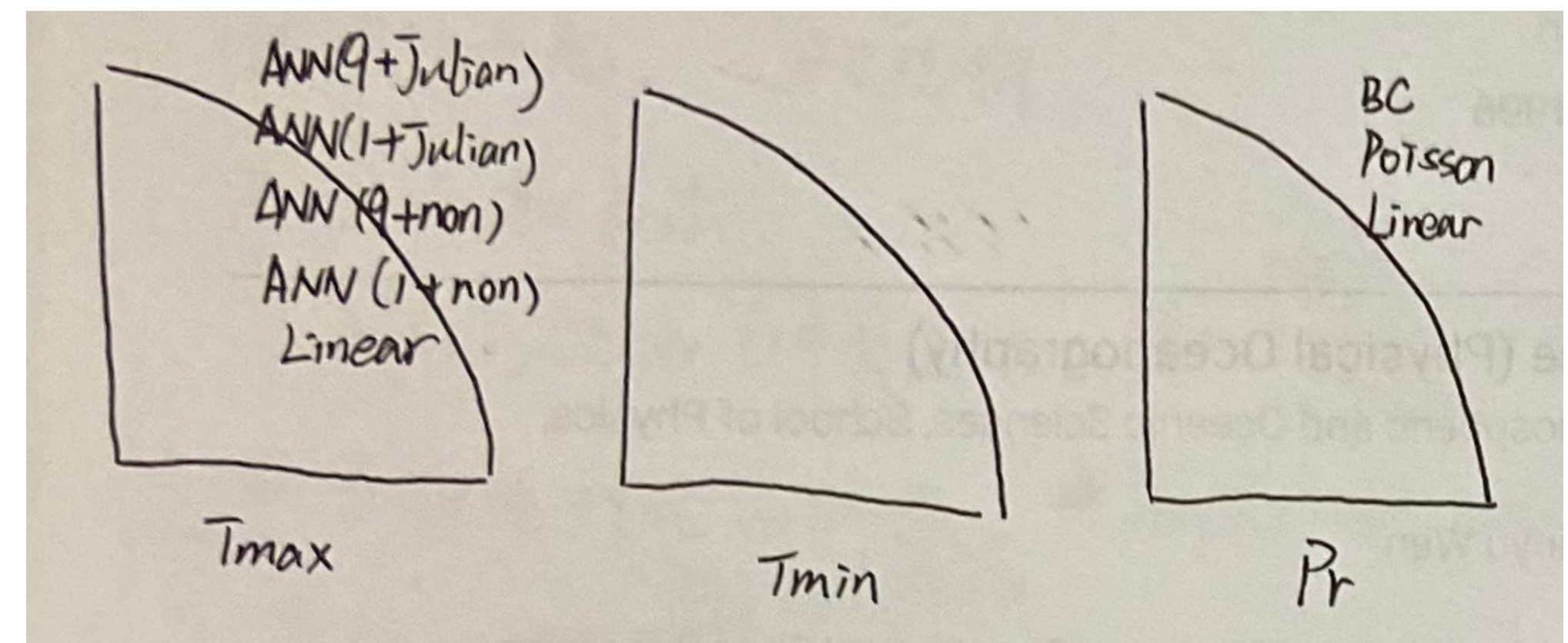


图4 历史阶段数据对比地图（中国）

Fig. 5 The Comparison of Historical Period in Map (China)

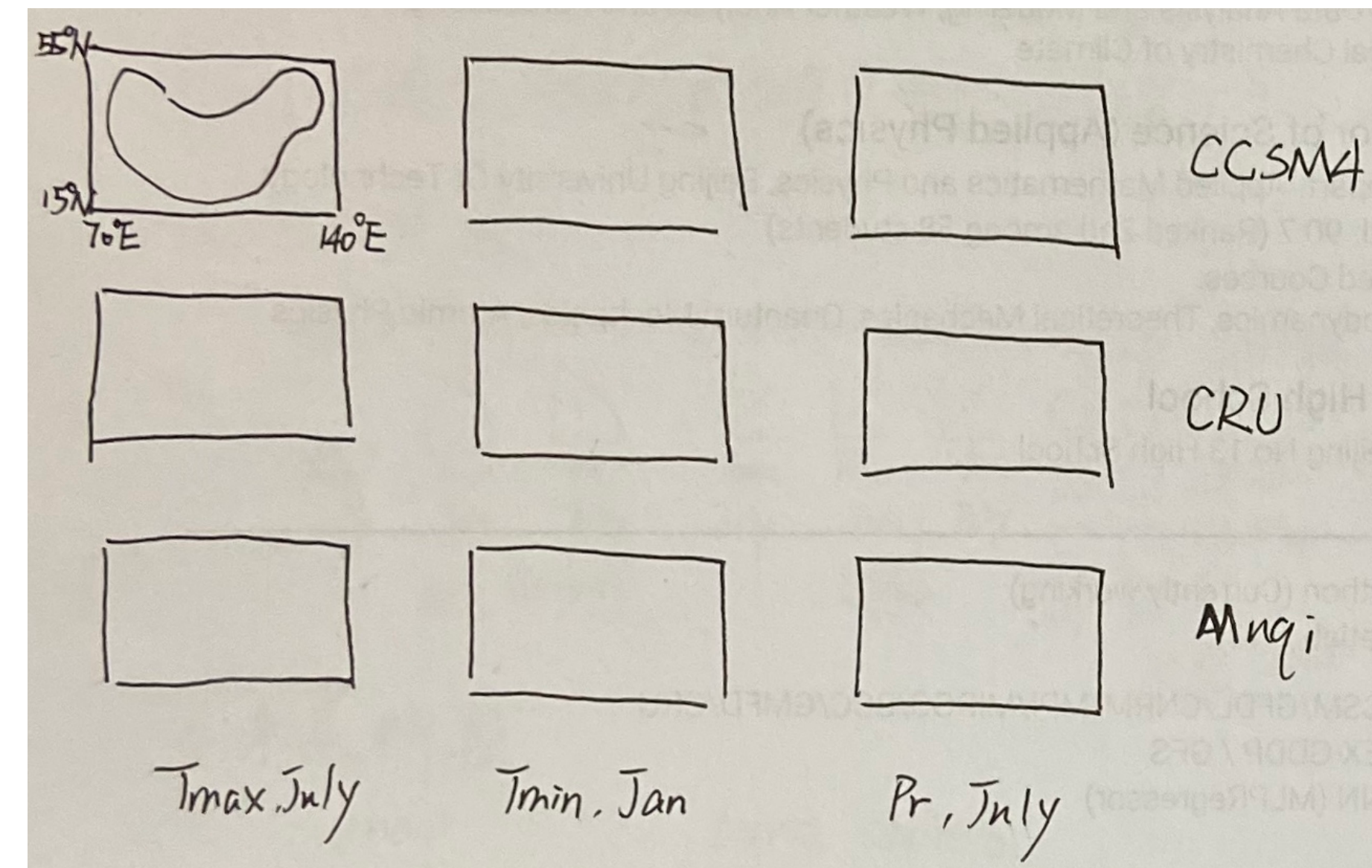
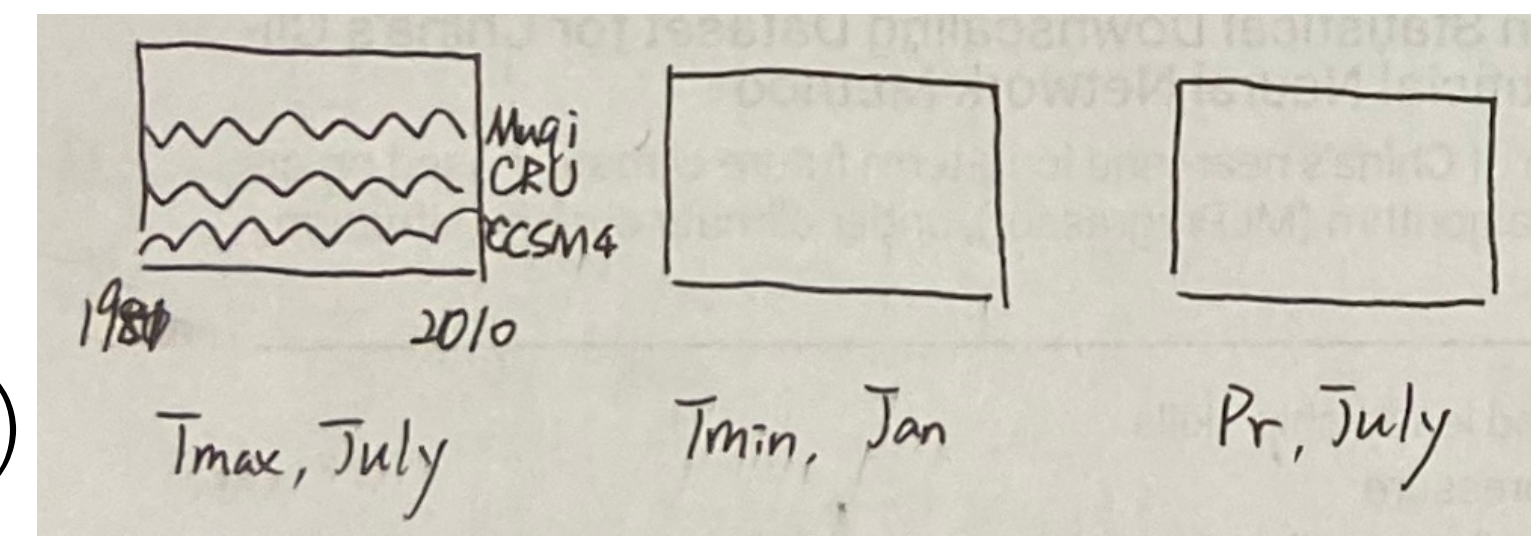


图5 历史阶段时间序列（中国）

Fig. 6 The Comparison of Historical Period in Time Series (China)



	Tmax		Tmin		
	obs	Mugí	obs	Mugí	
mean					
std					
r ²					
rmse					
	train		validation		

表1 日最高温和日最低温在训练集和验证集上的表现（中国）
 Table 1 The Quartiles during Train and Validation of
 Tmax and Tmin (China)

表2 日降水表现（中国）
 Table 2 The Quartiles of Pr (China)

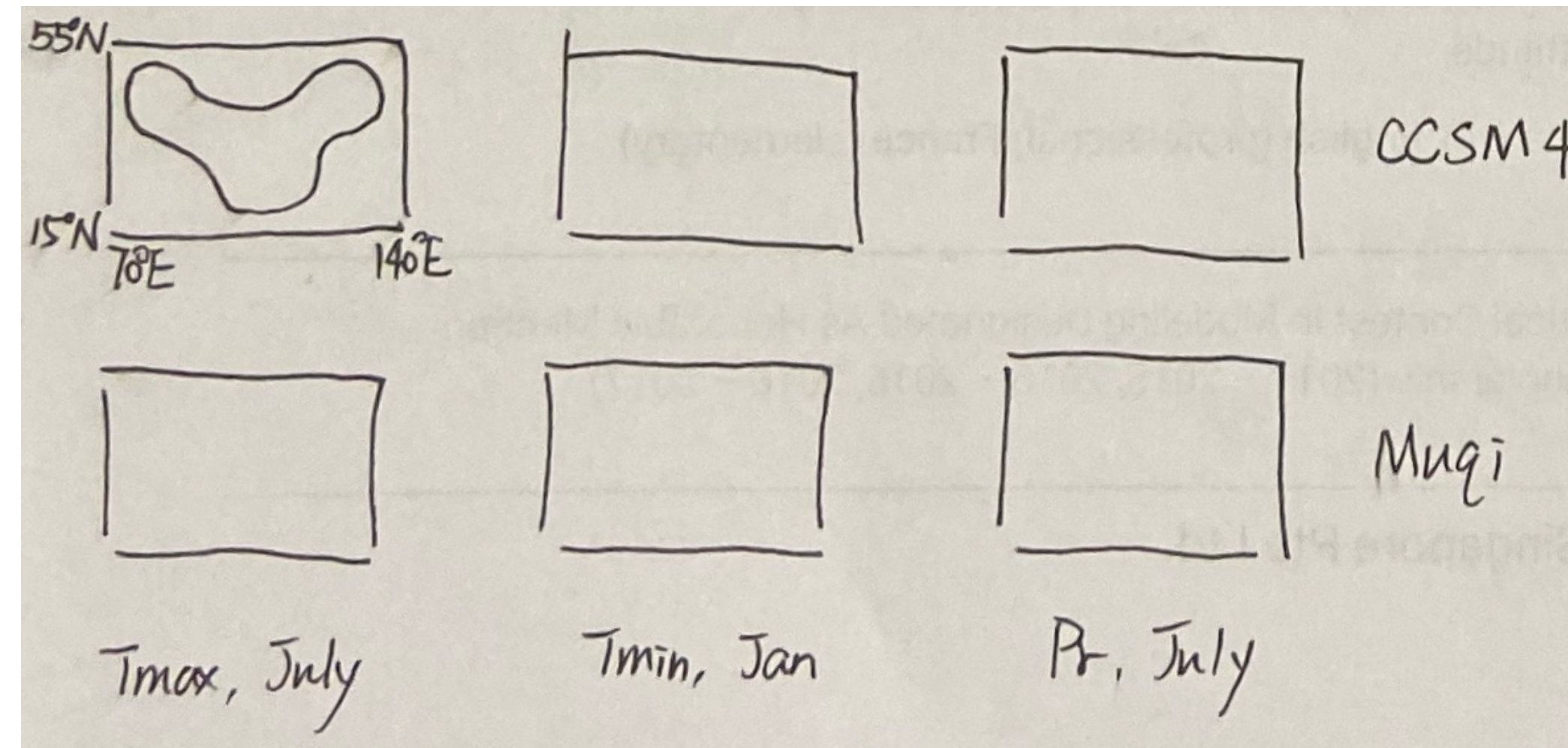


图6 RCP2.6情景短期未来数据对比

Fig. 6 The Comparison of Near-term Future in Map (RCP2.6)

图7 RCP2.6情景长期未来数据对比

Fig. 7 The Comparison of Long-term Future in Map (RCP2.6)

图8 RCP8.5情景短期未来数据对比

Fig. 8 The Comparison of Near-term Future in Map (RCP8.5)

图9 RCP8.5情景长期未来数据对比

Fig. 9 The Comparison of Long-term Future in Map (RCP8.5)

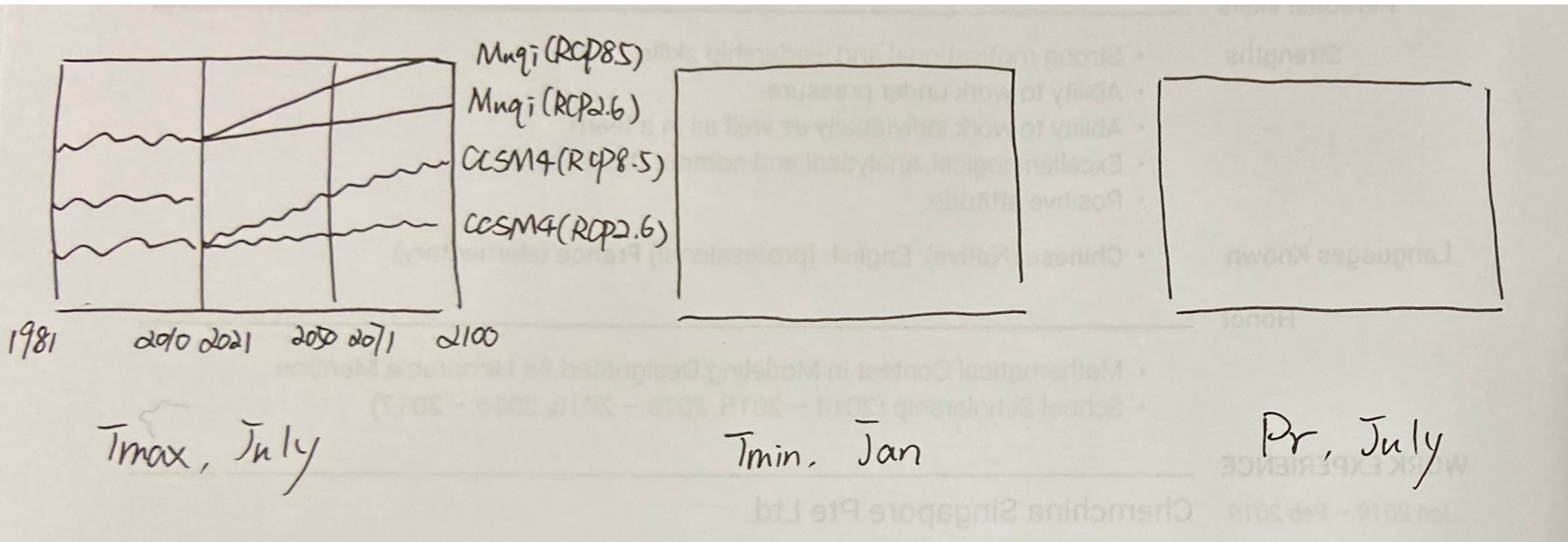


图10 气候变化（中国）
Fig. 10 Climate Change (China)

謝謝